CREATION OF A MATHEMATICAL MODEL ALLOWING QUALITATIVE AND QUANTITATIVE PREDICTION OF THE DISPERSION OF THE RESULTING REFRACTORY METAL POWDER

Alisher Rasulov, Fotima Umirzaqova, Shakhlo Abdulkhaqova, Shemshat Arazberdiyeva, Shokhrukh Tlovoldiyev
[1]Tashkent State Technical University
Email: alisher.rasulov@tdtu.uz

Abstract - The article discusses the results of a study to create a mathematical model that allows qualitatively and quantitatively predicting the dispersion of the resulting refractory metal powder, which suggests that the creation of a more advanced mathematical model for studying the process is currently real. An experimental laboratory plasma setup with a power of up to 20 kW is presented. It is shown that one of the main objectives of the work was to develop a mathematical model and technology for producing a sintered powder alloy of the Mo-TiC-Ni-W-Fe system. In order to improve the technological and operational characteristics of the experimental laboratory plasma setup, a rod tungsten cathode with a diameter of 5 mm, pressed into a copper water-cooled holder, is proposed to be used in the plasma torch. To ensure uniform feedstock supply, its rapid start and stop, a dispenser design created by the authors was used, operating on the principle of communicating vessels.

Keywords: Mathematical model, Powder, Dispersion, Refractory metal, Plasma-chemical reduction, Plasma jet, Mixing of raw materials, Alloy, Sintering.

1. Introduction

The creation of a mathematical model that allows qualitatively and quantitatively predicting the dispersion of the resulting refractory metal powder and establishing effective methods for its regulation requires the use of an integrated approach, i.e. reflecting the development of the process in the simultaneous and interconnected flow of all the main stages and phenomena [1].

The results of the study of theoretical and technological bases for creating a carbide tool with an optimal combination of strength and plasticity using highly dispersed powders of refractory metals are presented. It is shown that important technological aspects of creating carbide tools include obtaining powders of refractory metals by the method of plasma-chemical reduction of oxides of refractory metals.

The production of metals and the reductive synthesis of their compounds with carbon, nitrogen, boron, and silicon open up much broader possibilities for the use of low-temperature plasma. This is due not only to the wide range of types of raw materials and products, but also to smaller production volumes and increased requirements for its environmental friendliness [2-3].

All variants of existing plasma reduction units in this area can be divided into two main groups: in the first, the processes occur in a liquid bath (Fig. 1) with a shaft-type plasma gasifier of the melt. In the second, the formation of the target product is carried out in a gas-dispersed flow when mixing it with a plasma jet. In both cases, the raw material can be introduced into the high-temperature zone of the device in the form of vapors, melt, solution or powder of the required dispersion [9, 11]. Plasma furnaces with a ceramic bath are sufficiently versatile and therefore many of them, tested in ferrous metallurgy, are successfully used to produce non-ferrous metals such as nickel, cobalt, magnesium, vanadium, molybdenum, tin, tungsten, etc.

The tasks of industrial development of jet-plasma production of refractory metal powders require improvement of models, in particular, by describing technical variants of process implementation that are practically important in terms of equipment [10]. The relevance of the task is caused by the fact that until now the process has been modeled for the most impractical channel mode of plasma jet flow and only for the case of complete and instantaneous mixing of reagents. Fig. 1 and 2 show the flow diagrams of the plasma jet process. For ease of consideration and unification, the diagrams are divided into two autonomous modules. The first 5 flow diagrams of the plasma jet (Fig. 1) include the

most practical diagrams with its free and limited propagation [4].

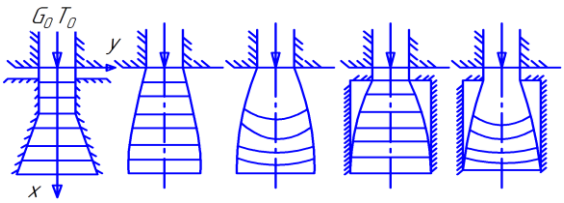

Figure 1: Plasma jet flow patterns: a) channel; b) free; c) limited; d) one-dimensional; d) two-dimensional

The second module presents 5 diagrams of the input and mixing of raw materials (Fig. 2): when using arc plasma torches, diagram 1 is typical, VCh plasma torches or multi-jet reactors – diagrams 2 and 3, additional diagrams 4 and 5 simulate the implementation of the process under conditions of intensive mixing of reagents behind the nozzle cut or in the plasma torch nozzle itself.

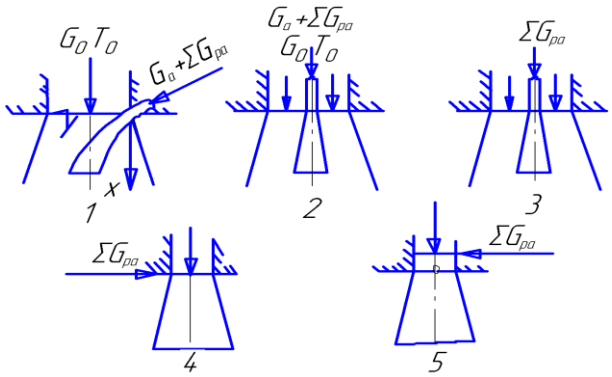

Figure 2: Scheme of raw material input and mixing: side input with TG (1), coaxial input with TG (2) and without TG (3), instantaneous mixing of raw material with plasma gas at the exit (4) and inside (5) the plasma torch nozzle

Thus, the proposed catalog of model process schemes covers 25 variants of its implementation. However, due to the need to use a one-dimensional description of the product condensation stage and, as a consequence, the stages of raw material processing, a two-dimensional model of plasma jet flow was used only for schemes with local input of raw materials. As a result, the number of process schemes considered by the author was reduced to 21, but they also largely reflect the actually feasible variety of process implementation options [5-6].

The difficulties of modeling this problem are caused, firstly, by the presence in the mixing zone of significantly non-uniform spatial distributions of temperature and gas velocity, secondly, by the insufficient development of the theory of nonequilibrium motion of free dispersed jets, and thirdly, by the absence in the literature of equations for predicting the trajectory of motion, drifting to a two-phase jet of carrier gas. Taking into account the complexities of the general formulation of the problem of determining the parameters of gas in the mixing zone, non-uniformities in the jet of carrier gas (CG) were identified with those in an axisymmetric single-phase turbulent self-similar jet, propagating in the form of a turbid flow, and the calculation of the trajectory of the drifting jet of CG and raw materials was based on known expressions obtained for non-isothermal single-phase jets.

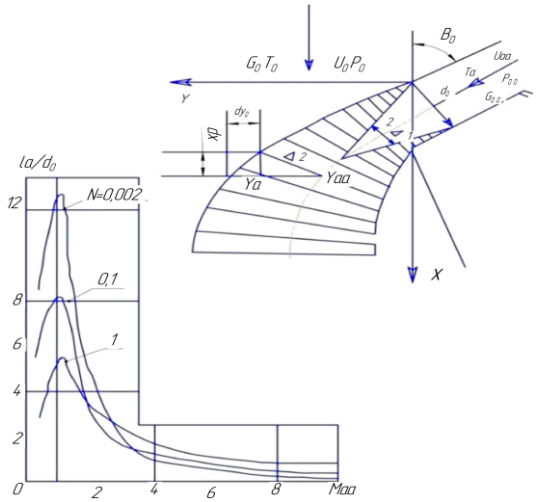

Figure 3: Scheme of lateral injection of TG jet into plasma flow

Some calculation results at $\Sigma G_{po} \to 0$ are shown in Fig. 5 and show that only the presence of TG leads to an increase of 1.5–5 times. The largest corrections are made for small particles, since when TG is neglected, they evaporate at flow lengths shorter than L_a (L_a=0,1 cm at U_{ao}=27m/s, L_a=0,4 cm at U_{ao}=82 m/s).

Calculations also showed that taking into account the presence of TG can provide an incomparably more accurate forecast of thermal, velocity and, as a consequence, concentration conditions at the early stage of product concentration, as well as predict the conditions of local cooling of the jet by raw materials.

Particles with a wide range of sizes from 10 to 100 μm can be used as raw materials for jet-plasma processing. It is possible to correctly track the change in their size during evaporation based on a sequential calculation, in the general case for all 3 modes characteristic of the Caudes number: diffusion, transition and kinetic.

2. The Proposed Mathematical Model

For a specific calculation of the movement of a drifting jet, one of the most general approximations was chosen.

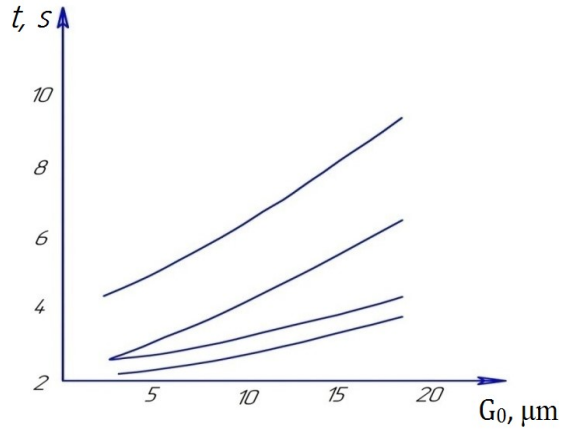

Figure 4: Time and length of the evaporation sections of polydisperse MoO3 particles, taking into account (1.2) and (3.4) mixing at Uao= 27 m/s (2.3) and 82 m/s

In the Cartesian coordinate system, it has the form:

$$\frac{x}{da} = 0.573\left(\frac{Y_a}{d_a}\right)1.818\cdot\left(\frac{S_n U_n^2}{S_a U_a^2}\right)^{0.754}\left(\frac{T_a}{T_0}\right)^{0.55} + \frac{Y_a}{d_a}Ctg\beta_a \quad (1)$$

where, S_n – cross-sectional area of the outgoing gas flow (cm^2); S_a – ordinate of the cross-sectional area of the outgoing gas flow; U^2_n – speed of the nozzle exit axis part (cm/s); U^2_a – ordinate of the velocity of the nozzle exit axis part (cm/s); d_a – diameter of the nozzle for input of raw materials (mm); T_0 – initial flow temperature; T_a – gas-plasma flow temperature; Y_a – coordinate of the leading edge of the related jet (cm); Y_a – ordinate of its axis (cm); $Ctg\beta_a$ – coal input and feed of raw materials into the reactor.

Known calculation methods are based on the adoption of a diffusion mechanism of the process or its correction is used with corrections for the rarefaction of the medium, obtained without taking into account mass transfer in the boundary layer of the particle.

According to the obtained results, the correction for the rarefaction of the medium - F_r., (equation 2) obtained without taking into account the mass transfer in the particle boundary layer, even in comparison with the well-known Kavanaugh correction, gives an increase of 3–7 times in the case of using hydrogen.

Fig. 5 shows the data of numerical calculations of the evaporation of MoO_3 particles in isothermal channel jets of Ar and H_2 (T = 3000 and 3500 °K, T_{pb} = 2207 °K, Q_p = I85 cal/g (specific heat of evaporation), α_u = I (evaporation coefficient of the substance), β_p = 1 (the number of molecules in the raw material particle, G_{Ar} = 2.5; G_{H2} = 0,I; U_{po} = 900; d_R = I + 0.44), F is the number of condensate fractions, $C_{p.p}$ is the specific heat capacity (cal/g·°K), K is the Boltzmann constant, M is the molecular weight (g/mol), Π is the channel perimeter (cm).

The evaporation of the particle was considered complete when its radius became less than 0.01 μm.

$$\phi_p = [1 + \frac{\alpha_p^{(o)}\beta_p}{\alpha_u Q_p p}\left(\frac{y}{c_{p,p}} - T_{p6}\right)\left(\frac{2\pi K T_{p6}}{M_g}\right)^{1/2}(1 + \Pi_4)]^{-1} \quad (2)$$

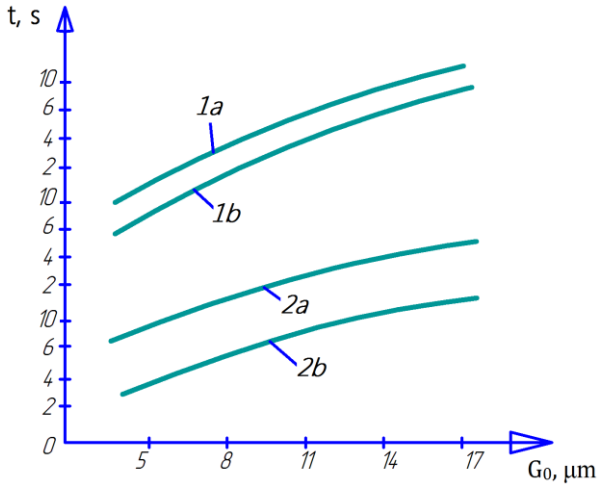

Figure 5: Evaporation time of MoO3 particles of different sizes at 30,000 (a) and 35,000 (b) in argon (1) and hydrogen (2) jets, taking into account the rarefaction of the medium according to the Kavanaugh expression

Plasma reduction of molybdenum oxide vapors in a hydrogen-containing flow occurs under conditions where even the value of T_0 is almost 2 times less than the metal condensation temperature. As a result, the intensity of condensation increases at supersaturation degrees reaching hundreds of units and more. If we add to this the presence of a nonlinear vapor source in the system and significant temperature and velocity gradients in the plasma jet, as well as the possibility of rapid depletion of the monovapor (due to high supersaturation) and the transition to coagulation growth of particles, then the incorrectness of the well-known and widely used method in calculations, based on the classical theory of enucleation, becomes obvious.

More reliable is the application of the coagulation mechanism developed in the works of Sutugin A.G. and co-workers in relation to the formation of condensate at extremely high steam saturations and rapidly changing external conditions.

Thus, the creation of a mathematical model that allows qualitatively and quantitatively predicting the dispersion of the resulting metal powder and establishing effective methods for its regulation requires the use of an integrated approach, i.e. reflecting the development of the process in the simultaneous and interconnected flow of all the main stages and phenomena [7-8].

Achieving this goal requires a revision of existing models of the stages of processing dispersed raw

materials. Certain requirements for their creation cause them to be built without taking into account the polydispersity of the raw materials and in relation to the conditions of the practically unheard-of implementation of the process with the channel flow of the plasma arc. However, a more serious discrepancy between the model and real conditions is the unresolved nature of the following issues:

1. All mathematical descriptions without exception are presented under the assumption of instantaneous and complete mixing of the dispersed raw material and the gas transporting it with the plasma flow. Meanwhile, it is well known that mixing cold gas with heated gas is characterized by low efficiency. The presence of dispersed material causes an additional slowdown in mixing. Finally, neglecting the separation of the reaction volume of the plasma jet from its total volume a priori gives unacceptable errors in calculating the condensation of the product.
2. There are absolutely no methods for calculating particle evaporation in the transition mode in the literature. The predicted evolution of the sizes of evaporating raw material particles should be recognized as unreliable without using such a method in the calculations. The consequence of this will be the unreliability of the predicted zones of raw material evaporation, changes in the concentrations of product vapors, and the deposition of the latter on the particles of the raw material.
3. The degree of negative influence of low-frequency pulsations of T_0 on processing of raw materials is unknown. The additional necessity of its determination indicates that with the help of this factor it is possible to control the choice of the electric power source of the plasma torch.

A review of the literature on the issues under consideration showed that the creation of a more advanced model for studying the process is currently feasible.

A description of a mathematical model free of the above-mentioned shortcomings, as well as the results of its numerical testing on a computer, comprise the content of this part of the work.

3. Research Objects and Methodology

A laboratory setup with a capacity of up to 20 kW for obtaining highly dispersed powders of refractory metals is shown in Fig. 6. The plasma torch used a rod tungsten cathode with a diameter of 5 mm, pressed into a copper water-cooled holder. The anode was a water-cooled copper nozzle with a diameter of 5 - 12 mm. The diameter of the graphite reactor is 90 mm, its length is 210 mm.

To ensure uniform feed of raw materials, its rapid start and stop, the author's design of the dispenser (Fig. 7) was used, operating on the principle of communicating vessels. The feedstock consumption was regulated by the number of revolutions of the hopper and the angle of its inclination and amounted to 0.005–0.1 g/s (with a thin-walled pipe with an external diameter of 5 mm, an internal diameter of 3 mm and its 40 mm).

In the experiments, a remote filter with a working surface of 0.5 m2 made of fiberglass was used. The plasma torch was supplied with gas from standard cylinders.

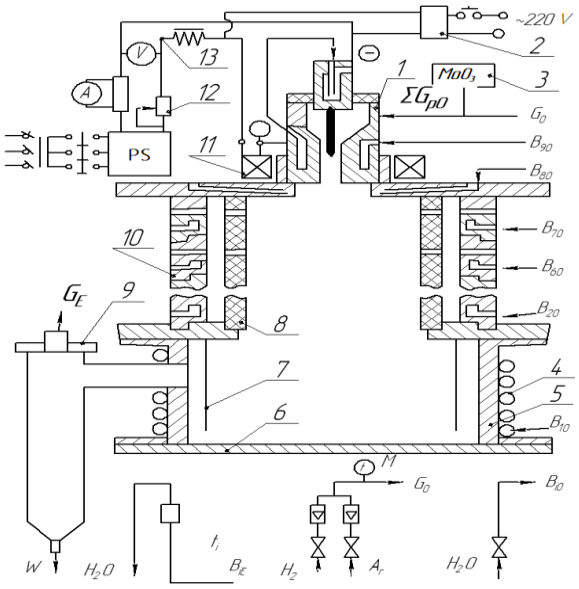

Figure 6: Laboratory setup diagram: 1 – plasma torch; 2 – oscillator; 3 – dispenser; 4 – coil; 5 – separator; 6 – separator bottom; 7 – deflector; 8 – heat shield; 9 – filter; 10 – reactor section; 11 – solenoid; 12 – rheostat; 13 – throttle; IP – power supply

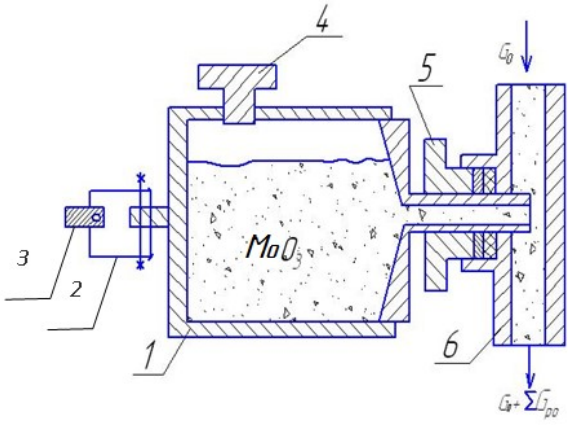

Figure 7: Schematic diagram of the dosing device: 1 - dosing hopper; 2 - cardan; 3 - motor shaft; 4 - plug; 5 - clamping nut; 6 - mixer

The plasma-forming gas was mainly a mixture of Ar and H_2. By mixing Ar, the 2-3-hour operating mode of the plasmatron without noticeable erosion of the electrodes, as well as the subsequent reproducibility of the operating modes of the installation, was achieved, which is necessary for complex studies.

The design of the feeder was selected based on testing a batcher with a stirrer (volume flow rate of raw materials G_{po} <30 kg/h), a feeder bin with a pseudo-chemical layer (G_{po}> 20 kg/h) and a feeder with a vertical screw. The best results in terms of pulsation level, reproducibility, and flow rate range were obtained with a screw feeder.

4. Research Results and Analysis

Preliminary study of 3-4 gas-dynamic and temperature fields in the reactor and their comparison with the calculated ones showed that: 1) the experimental velocity of plasma jets is 1.5-4 times less than the calculated one due to the outgoing flow, the influence of residual swirling of the plasma gas and the buffer zone (I_m-0, T_m=congt) in the lower part of the reactor, which occurs in the presence of a filtering surface at the gas outlet from the installation; 2) plasma jets are limited; 3) the use of a thermal screen evens out the radial temperature profiles and increases its values by 200-500.

Experiments with WO_3 processing were carried out using a graphite heat shield. Based on the analysis of the origin of the product accumulated at various units of the installation, the powder concentrating on the filter was used for experimental verification of the tungsten powder formation model. The values of S_{ud} determined by the BET method for nitrogen adsorption were used as an integral characteristic of the product dispersion. Preliminary experiments with quenching - dilution of the plasma flow with cold Ar at various distances *xfr* relative to the end of the cathode, determined the upper estimate of the temperature T_m = 1450 + 100, at which the fusion-sintering of tungsten particles in the plasma flow practically ends. The lower estimate was 1170 °K.

Table 1. Basic properties of tungsten carbide and cobalt

Properties	Tungsten carbide	Cobalt
Crystal lattice type is face-centered	α– hexagonal β– cubic, face-centered	α– hexagonal close packed β – cubic
Normal modulus of elasticity E at 290 °C kg/mm^2	72200	21500
Poisson's ratio	0,2	0,32
Microhardness at 290 K, load 50–200 kg/mm^2	2100	170
Tensile strength at 290 K, kg/mm^2 under compression	245	125
In bending, kg/mm^2	55	–
In stretching, kg/mm^2	35	77–88
Melting temperature, °K	3048	1758
Thermal conductivity, cal/cm.s. deg	0,05	0,155
Thermal coefficient of linear expansion, 10^{-5}/deg	4,4	14,2
Specific electrical resistance at 298 K, ohm/m	25	5,8

The calculation of the experiments on the synthesis of the model was carried out under the assumption that: 1) the raw material consists of three fractions with particle sizes of 10, 30 and 50 μm and their content of 3, 42, 55 mass. % (see Table 1); 2) the plasma flow is limited; 3) the axial distribution of temperature $T_m(x)$ in the plasma jet was specified according to experimental data with a maximum error of +100; 4) the calculation of the condensation-coagulation stage was carried out at a value of S_k equal to the density of liquid tungsten - 15.54 cm; 5) the change in S_{ud} of the product in the flow ceases at $T_m(x)$ < 1450 °K.

The design of the feeder for raw materials was selected based on testing of a batcher with a stirrer (G_{po}<30 kg/h), a feeder bin with a pseudo-chemical layer (G_{po}>20 kg/h) and a feeder with a vertical screw. The best results in terms of pulsation level, reproducibility, and flow rate range were obtained with a screw feeder.

5. Conclusions

The solubility of tungsten in cobalt depends to a large extent on the amount of carbon in the alloy and the cooling regime after sintering: in the case of a carbon deficiency, a high cooling rate leads to a significant increase in the tungsten content in cobalt.

Naturally, the presence of a certain amount of tungsten and carbon in the binding phase of WC–Co alloys leads to a change in its properties. This makes it possible to regulate the mechanical characteristics of hard alloys as a whole.

Thus, the possibilities of creating a mathematical model that allows qualitatively and quantitatively predicting the dispersion of the resulting refractory metal powder are theoretically substantiated.

References

[1] Shakirov Shukhrat, Bektemirov Begali, Sadaddinova Sanobar, Umirov Ulugbek, Tilavov Yunus. (2024). Mathematical modeling concerning ceramic compaction during a clay mass pressing process. International Journal of Mechatronics and Applied Mechanics, Volume 2024, Issue 15, Pp: 172 – 178, 2024. doi: 10.17683/ijomam/issue15.13

[2] Patent №IAP 04732. 26.06.2013. Nurmurodov S.D., Rasulov A.X. i dr. Plazmoximicheskiy reaktor [Plasma chemical reactor].

[3] Svetkov, Y.V., Samoxin, A.V. (2009). Plazmennaya nanoporoshkovaya metallurgiya [Plasma nanopowder metallurgy], "Mir Texniki i Texnologiy", №7 (2009)., Pp: 40 - 43.

[4] Kalamazov, R.U. (2004). Nanokristallicheskie strukturы v materialovedenii [Nanocrystalline structures in materials science]. Tashkent: TashGTU, 2004. Pp: 98.

[5] Samokhin, A.V., Alexeev, N.V., Kornev, S.A., Tsvetkov, Y.V. (2009). W-C nanosized composition synthesis and characterization, 19th International Symposium on Plasma Chemistry (ISPC-19), Bochum, Germany, July, Pp: 25-31, 2009.

[6] Nurmurodov, S.D., Rasulov, A.X. (2015). Sozdanie konstruksionnыx materialov s ispolzovaniem ultradispersnыx poroshkov volframa [Creation of structural materials using ultra-dispersed tungsten powders]: Monografiya, Tashkent, TashGTU, 2015. Pp: 168.

[7] Nurmurodov, S.D., Rasulov A.X. (2016). Ekstremal sharoitlarda ishlatiladigan qattiq qotishmali metall kompozitlar va ularni termik ishlash [Hard alloy metal composites used in extreme conditions and their thermal treatment]. Monografiya - Toshkent, ToshDTU, «Fan va texnologiya» nashriyoti, 2016. – Pp: 170.

[8] Rasulov, A.X. (2015). Ekstremal sharoitda ishlaydigan Mo-Tic-Ni-W-Fe sistemali qotishmalardan asboblar ishlab chiqarish texnologiyasini tadbiq qilish [Application of tool manufacturing technology from Mo-Tic-Ni-W-Fe system alloys working in extreme conditions]. Vestnik TashGTU. –Tashkent, 2015, №2. Pp: 160–164.

[9] Rasulov, A.X. (2016). Razrabotka texnologii proizvodstva novogo spechennogo splava Mo-TiC [Development of technology for the production of a new sintered alloy Mo-TiC]. Materialы V Mejdunarodnoy studencheskoy nauchno-prakticheskoy konferensii. Omsk, 4-10 aprelya 2016. Pp: 138-142.

[10] Alikulov Adkham, Bektemirov Begali, Begatov Jakhongir, Madaliyev Shukhrat, Yakubova Makhmuda. (2024). THE EFFECT OF CHROMIUM CONTENT AND PARAMETERS OF PRESSING AND SINTERING ON PROPERTIES OF Cu-Cr POWDER COMPOSITION. International Journal of Mechatronics and Applied Mechanics, Volume 2024, Issue 15, Pp: 172 – 178, 2024. doi: 10.17683/ijomam/issue15.20

[11] Karimov Shoirdjan, Shakirov Shukhrat, Bektemirov Begali, Sadaddinova Sanobar, Berdiyev Darob, Abdullaev Bekzod. (2024). CALCULATION OF THERMODYNAMIC INDICATORS OF THE POWDER COATING PROCESS IN A GAS FLAME. International Journal of Mechatronics and Applied Mechanics, Volume 2024, Issue 15, Pp: 172 – 178, 2024. doi: 10.17683/ijomam/issue15.7